NEURAL REGENERATION RESEARCH
www.nrronline.org

Research Article

A novel aged mouse model of recurrent intracerebral hemorrhage in the bilateral striatum

Li-Min Wang[1, 2], Zhi-Hua Liu[3], Hong-Lei Ren[4], Xue-Mei Chen[5], Jun-Min Wang[5], Hui-Min Cai[2], Li-Ping Wei[2], Hui-Hong Tian[2], Jian Wang[5, *], Li-Juan Wang[1, 2, *]

https://doi.org/10.4103/1673-5374.346459

Date of submission: October 23, 2021

Date of decision: January 7, 2022

Date of acceptance: April 19, 2022

Date of web publication: June 2, 2022

From the Contents

Introduction	344
Methods	345
Results	346
Discussion	347

Graphical Abstract

Behavior changes in a two-stage bilateral mouse model of striatal recurrent hemorrhage

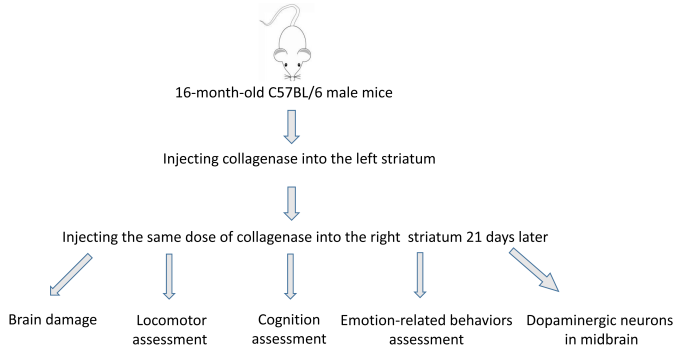

Abstract

The current animal models of stroke primarily model a single intracerebral hemorrhage (ICH) attack, and there is a lack of a reliable model of recurrent ICH. In this study, we established 16-month-old C57BL/6 male mouse models of ICH by injecting collagenase VII-S into the left striatum. Twenty-one days later, we injected collagenase VII-S into the right striatum to simulate recurrent ICH. Our results showed that mice subjected to bilateral striatal hemorrhage had poorer neurological function at the early stage of hemorrhage, delayed recovery in locomotor function, motor coordination, and movement speed, and more obvious emotional and cognitive dysfunction than mice subjected to unilateral striatal hemorrhage. These findings indicate that mouse models of bilateral striatal hemorrhage can well simulate clinically common recurrent ICH. These models should be used as a novel tool for investigating the pathogenesis and treatment targets of recurrent ICH.

Key Words: animal model; cognition impairment; depression-like behavior; dopaminergic neurons; emotion; intracerebral hemorrhage; motor; neurologic function; recurrent intracerebral hemorrhage

Introduction

Intracerebral hemorrhage (ICH) is associated with a high morbidity and mortality. The 1-month case fatality of ICH has been attributed to primary and secondary brain injuries (SBIs) (Wang, 2010; He et al., 2017; Pinho et al., 2019; Ren et al., 2020; Deng et al., 2021; Zhang et al., 2022). ICH survivors suffer from neurologic deficits and cognitive and emotional disturbances (Caeiro et al., 2013; Planton et al., 2017; Chen et al., 2020; Shi et al., 2021). These outcomes have been associated with SBI and ICH recurrence (Zhang et al., 2017; Jia et al., 2021). Hypertensive angiopathy (HA) and cerebral amyloid angiopathy (CAA), which account for 78% to 88% of all cases of ICH, contribute to recurrent ICH (Vidale et al., 2016; Boulouis et al., 2017; Charidimou et al., 2017, 2019; Pinho et al., 2021). Recurrent ICH related to HA has been found to be localized in deep areas, which results from the rupture of degenerated arterioles induced by uncontrolled hypertension (Weimar et al., 2011). HA-associated recurrent ICH frequently occurs in the contralateral basal ganglia due to gliosis at the first bleeding site. Recurrent CAA-related ICH is predominantly superficial or lobar in location (Pasi et al., 2018). Studies on recurrent ICH have mainly focused on clinical observations, such as the risk factors, disease severity, and bleeding site, which limits our understanding of its pathogenesis. One study found that CAA-related ICH has an annual recurrence of 10.5% *versus* an HA-related ICH recurrence of 3.7% (Casolla et al., 2019). Another study revealed that the ganglionic-ganglionic type was the most common form of ICH recurrence (Wolf et al., 2016). However, given that the pathogenesis of the two recurrent ICH subtypes is different, treatment strategies are also disparate (Nakase et al., 2012; Jandke et al., 2018). Therefore, it is necessary to explore the pathogenesis of recurrent ICH.

Collagenase-induced ICH is the most commonly used experimental ICH model (Li and Wang, 2017). This model mimics ICH by targeting the unilateral striatum, and has been used to promote preclinical and translational research (Manaenko et al., 2011). However, there is not yet an animal model that simulates recurrent ICH. Research on recurrent ICH has been limited to clinical observations that focus on bleeding sites and pathogenesis classification (Veltkamp and Purrucker, 2017; Weimar and Kleine-Borgmann, 2017). HA-related recurrent ICH has been reported to occur in 11–41% of patients with ICH (Ye et al., 2018). Therefore, we established and characterized a double-side ICH model ((d)-ICH) in aged mice to mimic HA-related recurrent ICH, which is more common in older patients (Tsai et al., 2021).

SBI exacerbates ICH outcomes (Lan et al., 2017, 2019; Boltze et al., 2021) and affects the perihematomal tissue and remote brain regions. Substantia nigra injury ipsilateral to the original hemorrhage or ischemia in the basal ganglia has been reported (Imamura et al., 2003; Fan et al., 2013), and this has been associated with cognitive dysfunction, anxiety, anhedonia, and movement disorders (Aswendt et al., 2021; Yang et al., 2022). Few studies have investigated the relationship between SBI and ICH recurrence, and remote injury in the midbrain after recurrent ICH has not been investigated. Furthermore, the effect of ganglionic ICH on the dopaminergic system is unclear. Finally, the impact of recurrent ICH on motor, cognitive, and emotion-like behaviors is undetermined, which hinders further research and intervention.

[1]The Second School of Clinical Medicine, Southern Medical University, Guangzhou, Guangdong Province, China; [2]Department of Neurology, Guangdong Provincial People's Hospital, Guangdong Academy of Medical Sciences, Guangdong Neuroscience Institute, Guangzhou, Guangdong Province, China; [3]School of Medicine, South China University of Technology, Guangzhou, Guangdong Province, China; [4]Department of Neurology, Tianjin Neurological Institute, Tianjin Medical University General Hospital, Tianjin, China; [5]Department of Anatomy, School of Basic Medical Sciences, Zhengzhou University, Zhengzhou, Henan Province, China

***Correspondence to:** Jian Wang, PhD, jianwang2020@outlook.com; Li-Juan Wang, PhD, wljgd68@163.com.

https://orcid.org/0000-0001-6584-8617 (Li-Min Wang); https://orcid.org/0000-0003-2291-640X (Jian Wang)

Funding: *This work was supported by the Natural Science Foundation of Guangdong Province of China, No. 2018A030313427 and the Science and Technology Program of Guangzhou of China, No. 202002030393 (both to LMW).*

How to cite this article: *Wang LM, Liu ZH, Ren HL, Chen XM, Wang JM, Cai HM, Wei LP, Tian HH, Wang J, Wang LJ (2023) A novel aged mouse model of recurrent intracerebral hemorrhage in the bilateral striatum. Neural Regen Res 18(2):344-349.*

Drawing on our experience with ICH models, we established a two-stage bilateral model by administering sequential collagenase injections to the bilateral striatum of mice to mimic recurrent ganglionic-ganglionic ICH. We then characterized the behavioral performance and "remote" brain injury in mice subjected to this novel model. Our findings help to explore the pathogenesis and treatment strategies for recurrent ICH.

Methods

Animals

The animal protocol was approved by the Research Ethics Committee of Guangdong Provincial People's Hospital, Guangdong Academy of Medical Sciences (approval No. AEC: 2019831A) on December 10, 2019. In this study, 16-month-old C57BL/6 male mice (25–35 g; Beijing Vital River Laboratory Animal Technology Co., Ltd., Beijing, China; license No. SCXK (Jing) 2016-0011) were used to mimic the cerebrovascular condition of older people. All mice were raised in a temperature- and light-controlled environment in pathogen-free animal rooms. All experiments were designed and reported according to the Animal Research: Reporting of *In Vivo* Experiments (ARRIVE) guidelines (Percie du Sert et al., 2020). All efforts were made to minimize the suffering of the animals used. Based on our preliminary studies, a sample size estimation indicated that 8 mice/group would provide at least 80% power for detecting a 20% change in lesion volume at α = 0.05 (two-sided). Considering that the two-stage injection ICH model may result in high mortality, we used 15 mice/group. Animals that died during the operation were excluded from the analysis.

A total of 84 mice were used in this study. Mice were randomly assigned to the single-side ICH (s-ICH; *n* = 27), single-side sham control (s-control; *n* = 15), d-ICH (*n* = 27), and double-side sham control (d-control; *n* = 15) groups using the randomizer form at www.randomizer.org (Li et al., 2017b; Zhang et al., 2018). The flow chart is shown in **Figure 1**.

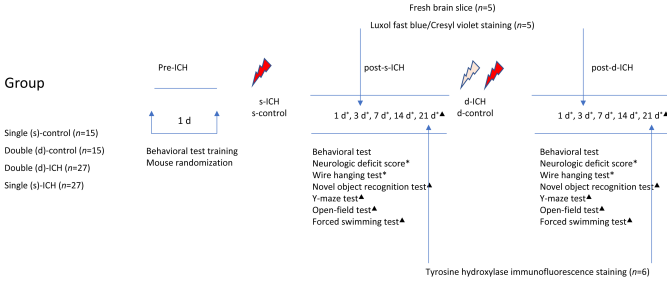

Figure 1 | **Study flow chart.**
ICH: Intracerebral hemorrhage.

s-ICH and d-ICH models

Mice were anesthetized with 3% isoflurane (Shanghai Yuyan Instruments Co. Ltd., Shanghai, China) for induction, then 1–2% isoflurane for maintenance. During the operation, an electronic thermostat-controlled warming blanket maintained the rectal temperature at 37 ± 0.5°C until mice recovered from anesthesia completely and performed normal motor activity (Han et al., 2019).

s-ICH

We injected 0.35 μL collagenase VII-S (0.075 U in 0.5 μL saline; MilliporeSigma, St. Louis, MO, USA) into the left striatum of mice (*n* = 27) at the following stereotactic coordinates: 0.6 mm anterior and 2.0 mm lateral to the bregma, and at a depth of 3.0 mm, as previously described (Han et al., 2019). We used a lower dose of collagenase than a former study (Li et al., 2017c), because of the use of older mice and the two-stage injection design. During surgery, three mice died from anesthesia, and two mice died from severe neurologic deficits on day one after the operation. Twenty-two mice with successful s-ICH were used in the subsequent experiments.

d-ICH

We established the d-ICH model in two stages. In stage one, we established the s-ICH model as described above. In stage two, 21 days after s-ICH, mice received a second 0.35 μL collagenase VII-S injection into the right striatum at the following stereotactic coordinates: 0.6 mm anterior and 2.0 mm lateral of the bregma, and at a depth of 3.0 mm. During surgery, one mouse died in stage one, and three mice died in stage two due to severe neurologic deficits. Twenty-three mice with successful d-ICH were used in the subsequent experiments.

s-control and d-control

We randomly selected 30 mice as the sham control group. The s-control group (*n* = 15) was injected with an equal volume of saline into the left striatum, and the injection coordinate parameters were the same as for the s-ICH group. Two mice died from anesthesia. The d-control group (*n* = 15) was treated in the same way as was the d-ICH group, with 0.35 μL normal saline injected into the left striatum in stage one, then 0.35 μL normal saline injected into the right striatum 21 days later in stage two. The two injection coordinate parameters were the same as those of the d-ICH mice.

Hematoma volume and lesion volume

Mice from the s-ICH and d-ICH groups (*n* = 10 mice/group) were sacrificed on day 3 after the operation. Five randomly selected brains were cut into 1 mm-thick fresh sections using a brain matrix. Another five brains in each group were cut into 60 μm-thick sections and stained with Luxol fast blue and Cresyl violet based on our established protocol (Chang et al., 2014). ImageJ software version 1.52a (National Institutes of Health, Bethesda, MD, USA; Schneider et al., 2012) was used to calculate the volume of the hematoma and lesion by multiplying the thickness by the sum of the damaged areas in each section (Yang et al., 2017).

Neurologic function

Neurologic deficit score

The neurologic deficits of mice were evaluated using a 24-point scoring test (Li et al., 2017a) on days 1, 3, 7, 14, and 21 after the operation. Using the scoring system, we scored the four groups on six parameters, including body symmetry, gait, climbing, circling behavior, front limb symmetry, and compulsory circling. Each test was graded from 0 to 4, resulting in a maximum deficit score of 24.

Wire hanging test

The wire hanging test (Zhu et al., 2014, 2018) was used to assess gripping and forelimb strength, coordination, and endurance, and was implemented on days 1, 3, 7, 14, and 21 after the operation. Mice were hung from the forelimbs on a 55-cm long iron wire (1 mm in diameter) between two posts that were 50 cm above the ground. We placed a pillow underneath the mice to prevent falling injuries. The hind limbs were gently covered by tape to prevent mice from using all four paws. The animals were trained before formal experiments, and the falling latency was recorded during assessments.

Novel object recognition test

The novel object recognition (NOR) test was used to evaluate recognition and initiative exploration on day 21 after the operation, as previously described (Zhu et al., 2014). Briefly, the NOR included three processes. First, mice were placed in an open field (47 cm × 26 cm × 20 cm) for 5 minutes on day 1 to habituate. Second, we placed two identical novel objects (green cubes, 4 cm × 4 cm × 3 cm) in the arena. The mice had 10 minutes to explore them on the day two training. After one hour of training, mice were exposed to a novel object (red scalene triangle, 5 cm in diameter) and a familiar object (green cube) for 5 minutes. A camera was used to record the whole test period. The time in direct contact within the object area was calculated as the time it took to explore an object. Sniffing or touching with the nose or forepaws within 0.5 cm around the object was defined as an exploration event. The discrimination index and total exploration time were calculated for each mouse. The discrimination index was used to assess cognitive ability (Zhu et al., 2014; Chen et al., 2020) and was calculated as follows: Discrimination index (%) = (time spent on novel object/total time devoted to exploring novel and familiar objects) × 100. Contacts judged as accidental, and standing, sitting, or leaning on the object were excluded. Meanwhile, the exploration duration (total time spent exploring the novel and familiar objects) was calculated to estimate exploring initiative of the mice.

Y-maze test

The Y-maze was used to assess short-term memory, spatial memory, and innate curiosity in mice (Chen et al., 2020; Shi et al., 2021). The maze was made of white painted wood. Each arm (marked as A, B, and C) was 30 cm long, 17 cm high, 10 cm wide, and positioned at equal angles. On day 21 after the operation, mice were placed in the middle of the maze and allowed to move freely for 5 minutes. A camera was used to record the number of arms entered and the alternations. When the whole body of the mouse completely went into an arm, we considered it an arm entry. When the mouse continuously passed a non-repeated entry into arms A, B, and C, we considered it a successful cycle (Miedel et al., 2017). The alternation was calculated as the ratio of successful processes by the number of adequate turns (defined as the total number of arm entries minus 2) multiplied by 100.

Open-field test

The open-field test was used to evaluate locomotor activity and anxiety-like behavior in the four groups on day 21 after the operation (Seibenhener and Wooten, 2015; Shi et al., 2021). We used a 50 cm × 50 cm × 38 cm square box without a cover. Its bottom was subdivided into 25 equal squares (nine squares in the "interzone" center, surrounded by 16 outer zones). The video recording device was connected to a computerized tracking system. We placed mice in the well-lit box, directly above which a video camera was mounted. The mice were placed in the open field center, allowing freedom of movement. The Viewer software (SMART v3.0-Panlab Harvard Apparatus, Shenzhen, China) was used to record the behavior of mice for 10 minutes in the box and analyze the activity of each mouse according to total distance traveled, average speed, and time spent in the center zone.

Forced swimming test

During the forced swimming test, mice were placed individually in a clear Perspex cylinder (20 cm high × 22 cm in diameter) filled to a depth of 15 cm with water that had a temperature of 25 ± 1°C. The movements of mice

on day 21 after the operation were recorded for 6 minutes using a camera. The absence of escape-oriented behaviors, such as swimming, jumping, rearing, sniffing, or diving, indicates behavioral despair. Mice floating upright and making only small movements to remain above water were considered immobile (Yankelevitch-Yahav et al., 2015; Shi et al., 2021). The immobility time during the final 4 minutes of the test was recorded.

Tyrosine hydroxylase immunofluorescence staining

Immunofluorescence of dopaminergic neurons in the midbrain was conducted as described previously (Han et al., 2016) to assess tyrosine hydrolase protein expression. Animals were anesthetized with 4% isoflurane and then perfused with ice-cold 0.1 M PBS (pH 7.4) and 4% paraformaldehyde. Brains were removed, post-fixed overnight in 4% paraformaldehyde, and then placed in 30% sucrose for 2 days. Fixed midbrain sections on day 21 after s-ICH or d-ICH were incubated overnight at 4°C with rabbit anti-tyrosine hydroxylase antibody (1:200, MilliporeSigma, Cat# ab137869, RRID: AB_373130), followed by Alexa 594 conjugated-goat anti-rabbit IgG (1:2000, Invitrogen, Eugene, OR, USA, Cat# A11007, RRID: AB_141374) at room temperature for 1 hour. From bregma, three 10-μm typical planes were selected at 2.70 mm, 3.52 mm, and 3.88 mm. Four to six photographs were taken from each layer, and the total number of dopaminergic neurons of the three selected layers was summed. The sections were observed under a Nikon Eclipse 90 immunofluorescence microscope (Nikon Co., Tokyo, Japan).

Statistical analysis

Mice that died during surgery or shortly after ICH were excluded from the final analysis. Investigators who were blinded to the four groups evaluated the behavioral and histologic outcomes of all mice and performed the data analysis. All data are presented as the mean ± standard deviation. Comparisons between two groups were made using unpaired *t*-tests. For behavioral tests, data at different time points for the same group were compared using one-way analysis of variance with a Dunnett's *post hoc* test. Data from other groups were simultaneously compared using a two-way analysis of variance with the Tukey *post hoc* test. Comparisons of mortality ratios were made using chi-square tests. Statistical analysis were performed using GraphPad Prism 8.0.2 (GraphPad Software, San Diego, CA, USA, www.graphpad.com). Between-group differences were considered statistically significant at $P < 0.05$.

Results

Mortality of the two-stage bilateral recurrent ICH in aged mice

The mortality of mice was 5 out of 27 (18%) in the s-ICH group, 4 out of 27 (15%) in the d-ICH group, 2 out of 15 (13%) in the s-control group, and 2 out of 15 (13%) in the d-control group. There was no difference in mortality between the four groups ($P > 0.05$).

Volume of hematoma and lesion in two-stage bilateral recurrent ICH in aged mice

Three days after surgery, the hematoma was present in both the s-ICH and d-ICH groups. Fresh brain sections were used to calculate the volume of the hematoma, and Luxol fast blue and Cresyl violet staining were used to quantify the lesion volume (**Figure 2A**). There were no significant differences in hematoma or lesion volume between the s-ICH and d-ICH groups (both, $P > 0.05$; **Figure 2B** and **C**).

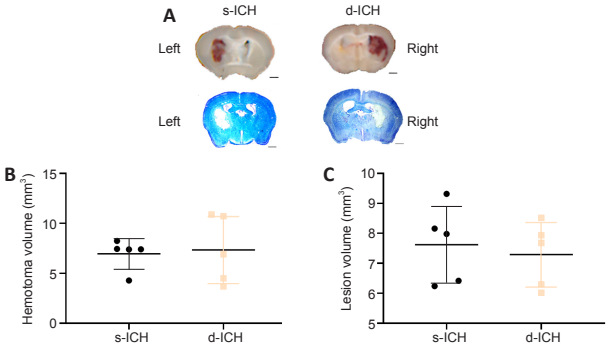

Figure 2 | Brain injury in a two-stage bilateral recurrent intracerebral hemorrhage aged mouse model on day 3 after surgery.

(A) Luxol fast blue images of fresh brain sections in the left striatum of the s-ICH group and right striatum of the d-ICH group. The hematoma was restricted to the striatum. Scale bars: 1 mm. (B) Quantification showed no differences in hematoma volume between the s-ICH and d-ICH groups ($P = 0.8204$). (C) Quantification showed no differences in lesion volume between the s-ICH and d-ICH groups on day 3 ($P = 0.6709$). All data are presented as dot plots with the mean ± SD ($n = 5$ mice/group), and were analyzed using two-way analysis of variance followed by Kruskal-Wallis *post hoc* tests. d-ICH: Two-stage bilateral intracerebral hemorrhage; s-ICH: single side intracerebral hemorrhage.

Changes of motor and cognitive function in two-stage bilateral recurrent ICH in aged mice

Neurologic deficit scores

Neurologic deficit scores in the s-ICH and d-ICH groups were higher than those of their respective controls on days 1, 3, 7, 14, and 21 ($n = 13$, $F = 8.987$, $P < 0.01$; **Figure 3A**). Only on day 14, the neurologic deficit scores were significantly higher in the d-ICH group than in the s-ICH group ($F = 18.46$, $P < 0.05$). The s-ICH and d-ICH groups exhibited gradual recovery from days 3 to 21.

Wire hanging test

In the wire hanging test, gripping, forelimb strength, coordination, and endurance were impaired in both the s-ICH and d-ICH groups on days 1, 3, 7, 14, and 21 compared with their respective controls ($n = 12$–13 mice, $F = 0.9723$, $P < 0.01$; **Figure 3B**). The falling latency was shorter in the d-ICH group than in the s-ICH group on days 3, 7, and 14 (all, $P < 0.05$). Meanwhile, both ICH groups' performance in the wire hanging test gradually recovered from days 3 to 21. On day 21, both the s-ICH and d-ICH group continued to show motor deficits compared to their sham controls (both, $P < 0.05$); nevertheless, the motor deficit was more severe in the d-ICH group than in the s-ICH group, except for on day 1 (all, $P < 0.05$).

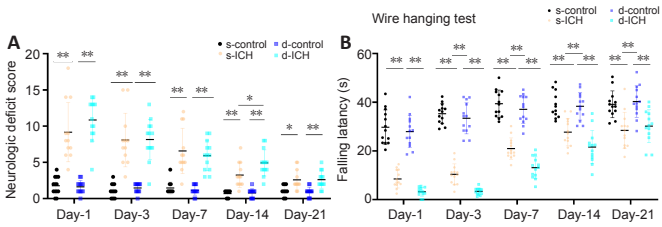

Figure 3 | Changes in neurologic deficit scores and falling latency over time in a two-stage bilateral recurrent intracerebral hemorrhage aged mouse model.

(A) Mice with s-ICH and d-ICH showed significantly higher neurologic deficit scores than their respective controls. Mice with d-ICH had a significantly higher neurologic deficit score than mice with s-ICH 14 days after the operation ($F = 18.46$, $P < 0.05$). Both the s-ICH and d-ICH groups showed gradual recovery from days 3 to 21 ($F = 8.987$, $P < 0.05$). (B) The falling latency was shorter in mice with s-ICH and d-ICH than their respective controls. The falling latency was significantly shorter in d-ICH mice than in s-ICH mice on days 3, 7, 14, and 21 ($F = 0.9723$, both, $P < 0.05$). All data are presented as dot plots with the mean ± SD ($n = 12$–13). *$P < 0.05$, **$P < 0.01$ (two-way analysis of variance followed by Kruskal-Wallis *post hoc* tests). d-ICH: Two-stage bilateral intracerebral hemorrhage; d-control: two-stage bilateral sham surgery; s-ICH: single side intracerebral hemorrhage; s-control: single side sham surgery.

Cognitive function test

In the NOR test, the discrimination index ($n = 12$–13, $F = 1.443$, $P < 0.01$; **Figure 4A**) and the exploration time ($n = 12$–13, $F = 0.5697$, $P < 0.011$; **Figure 4B**) of the s-ICH and d-ICH groups were significantly lower than their respective controls. The discrimination index and time to exploration of the d-ICH group were lower than those in the s-ICH group (both, $P < 0.05$).

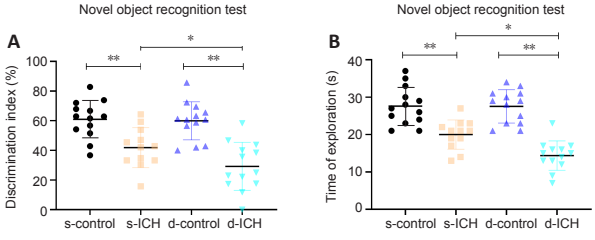

Figure 4 | Changes of cognitive function in a two-stage bilateral recurrent intracerebral hemorrhage aged mouse model.

(A, B) In the novel object recognition test, the discrimination index ($F = 1.443$, $P < 0.05$; A) and the total exploration time ($F = 0.5697$, $P < 0.001$; B) in mice with s-ICH or d-ICH were significantly lower/shorter than their respective controls. These two parameters were worse in d-ICH mice than in s-ICH mice (both, $P < 0.05$). All data are presented as dot plots with the mean ± SD ($n = 12$–13). *$P < 0.05$, **$P < 0.01$ (two-way analysis of variance followed by Kruskal-Wallis *post hoc* tests). d-ICH: Two-stage bilateral intracerebral hemorrhage; d-control: two-stage bilateral sham surgery; s-ICH: single side intracerebral hemorrhage; s-control: single side sham surgery.

In the Y-maze test, the alternation was significantly lower in both the s-ICH and d-ICH groups than in their respective controls ($n = 12$–13 mice/group, $F = 4.114$, $P < 0.05$; **Figure 5A**), and the d-ICH group exhibited fewer alternations than the s-ICH group ($P < 0.05$). There were no significant differences in alternation between the four groups ($F = 1.294$, $P > 0.05$; **Figure 5B**).

Locomotor and emotional behaviors

The typical movement track in the open field test for each group is shown in **Figure 6A**. Compared to their respective controls, the total distance traveled was shorter, and the average speed was slower in the s-ICH and d-ICH groups (both, $P < 0.05$; **Figure 6B** and **C**). These two parameters were much lower in the d-ICH group than in the s-ICH group ($P < 0.05$). However, the time spent

in the center zone was not significantly different between the four groups (n = 12–13, F = 0.9091, P > 0.05; **Figure 6D**).

In the forced swimming test, the immobility time in the s-ICH and d-ICH groups was significantly longer than that of their respective controls (both, P < 0.01). Immobility time was longer in the d-ICH group than in the s-ICH group (n = 12–13, F = 0.9591, P < 0.01; **Figure 6E**).

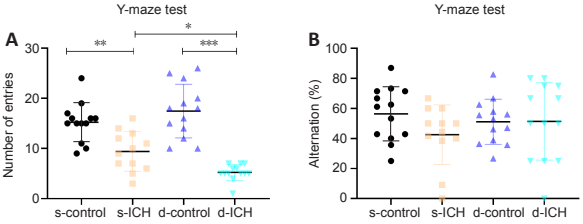

Figure 5 | Changes of spatial memory and initiative exploration in a two-stage bilateral recurrent intracerebral hemorrhage aged mouse model in the Y-maze test.
(A) The number of entries in s-ICH and d-ICH mice was smaller than their respective controls (F = 4.114, P < 0.05), with a significantly worse performance in d-ICH mice than in s-ICH mice. (B) There were no significant differences in alternation between the four groups (F = 1.294, all, P > 0.05). All data are presented as dot plots with the mean ± SD (n = 12–13). *P < 0.05, **P < 0.01, ***P < 0.001 (two-way analysis of variance followed by Kruskal-Wallis *post hoc* tests). d-ICH: Two-stage bilateral intracerebral hemorrhage; d-control: two-stage bilateral sham surgery; s-ICH: single side intracerebral hemorrhage; s-control: single side sham surgery.

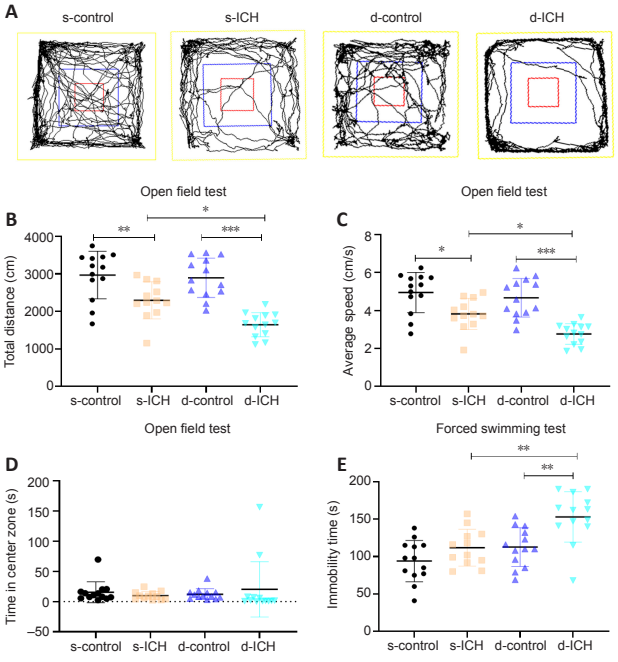

Figure 6 | Changes of locomotion and emotional behaviors in a two-stage bilateral recurrent intracerebral hemorrhage aged mouse model.
(A) The track of the movement of the open field test. (B) Within 10 minutes, the total distance traveled by s-ICH and d-ICH mice was shorter than their respective controls (n = 13, F = 1.2931, P < 0.01); moreover, the d-ICH mice traveled less distance than did the s-ICH mice (P < 0.01). (C) The average speed in mice with s-ICH and d-ICH was significantly slower than their respective controls (n = 12–13, F = 1.669, P < 0.05), and d-ICH mice were slower than s-ICH mice (P = 0.0227). (D) The time in the center zones did not differ between the four groups (n = 12–13, F = 0.9091, P > 0.05). (E) In the forced swimming test, immobility time was significantly longer in d-ICH mice than in their controls and s-ICH mice (n = 12–13, F = 0.9591, P < 0.01). s-ICH mice tended to have a longer immobility time than the s-control group, but this difference did not reach significance (P > 0.05). All data are presented as dot plots with the mean ± SD. *P < 0.05, **P < 0.01, ***P < 0.001 (two-way analysis of variance followed by Kruskal-Wallis *post hoc* tests). d-ICH: Two-stage bilateral intracerebral hemorrhage; d-control: two-stage bilateral sham surgery; s-ICH: single side intracerebral hemorrhage; s-control: single side sham surgery.

Changes in the number of dopaminergic neurons in the midbrain of two-stage bilateral recurrent ICH in aged mice

Tyrosine hydroxylase immunofluorescence staining was used to evaluate changes in the number of dopaminergic neurons in the midbrain on day 21 after s-ICH or d-ICH. Contrary to our expectations, there were no significant differences between the four groups (all P > 0.05). However, the s-ICH and d-ICH groups tended to have fewer dopaminergic neurons than their respective controls (n = 6, F = 1.802, P = 0.6370 and 0.1398, respectively; **Figure 7A** and **B**).

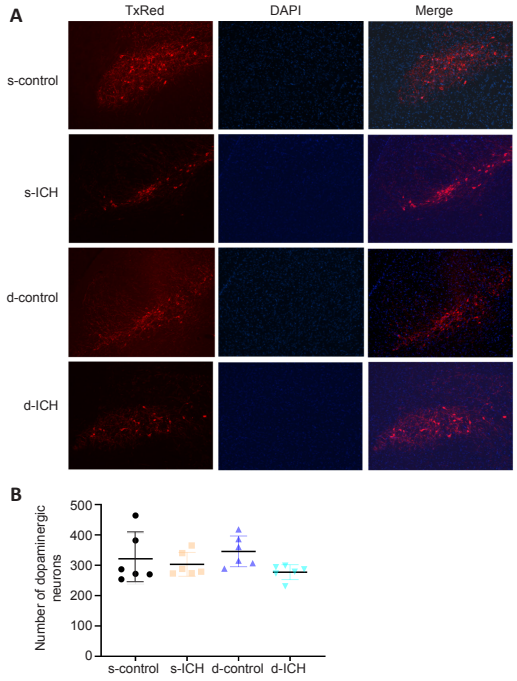

Figure 7 | Changes in the number of dopaminergic neurons in the midbrain in a two-stage bilateral recurrent intracerebral hemorrhage aged mouse model.
(A) Immunofluorescence staining with tyrosine hydroxylase (TH, red, Alexa 594) on day 21 after s-ICH or d-ICH. (B) The number of dopaminergic neurons did not differ significantly between the four groups, although it tended to be lower in d-ICH mice than in control mice (F = 1.802, P > 0.05). All data are presented as dot plots with the mean ± SD (n = 5) and were analyzed using one-way analysis of variance followed by Kruskal–Wallis *post hoc* tests. DAPI: 4′,6-Diamidino-2-phenylindole; d-ICH: two-stage bilateral intracerebral hemorrhage; d-control: two-stage bilateral sham surgery; s-ICH: single side intracerebral hemorrhage; s-control: single side sham surgery.

Discussion

In this study, we successfully established a novel two-stage bilateral mouse model of ICH to simulate recurrent ICH. We used aged animals to mimic the cerebrovascular effects of aging. This novel model generated reproducible hematoma, lesions, and neurologic deficits. It also produced marked memory and emotional deficits. Compared to s-ICH mice, d-ICH mice exhibited more severe neurologic deficits, memory dysfunction, and depression-like behaviors, closely mimicking the symptoms of recurrent ICH in clinics. Interestingly, we did not observe a significant loss of dopaminergic neurons in the midbrain in s-ICH or d-ICH mice. However, s-ICH and d-ICH mice tended to have fewer of these neurons than their respective controls. This could help us understand the pathogenesis of vascular Parkinsonism, which is characterized by dysfunction of the dopaminergic system rather than a reduced number of dopamine neurons, as is seen in Parkinson's disease.

We used a 24-point neurologic scoring system to evaluate overall locomotor function (Li et al., 2017a; Li and Wang, 2017), and the wire hanging test to assess grip strength, coordination, and forelimb endurance (Zhu et al., 2018). Both s-ICH and d-ICH mice exhibited marked motor deficits on days 1, 3, 7, 14, and 21 after ICH. The difference between the four groups gradually decreased over time, consistent with clinical signs/symptoms in patients with ICH whose neurologic function progressively improves when hematomas stabilize. Gripping and forelimb strength and coordination decreased in the s-ICH and d-ICH mice at the five-time points. d-ICH mice performed significantly worse than the s-ICH mice in this task, except for day one after ICH. The wire hanging test seems to be more sensitive to evaluate forelimb muscle coordination and endurance in the d-ICH model, with better performance than the neurologic scoring system. Consistent with this result, in the open field test, the average movement speed of d-ICH mice was slower and the total distance traveled within 10 minutes was shorter than s-ICH mice. Therefore, we concluded that d-ICH mice had more severe motor deficits in gripping and forelimb strength and coordination from days 3 to 21 after d-ICH. Augmented SBI due to locally produced proinflammatory mediators in response to repeated bleeding could explain this result. SBI developed around the hematoma and in brain regions that were remote from the hematoma. SBI affected the pyramidal tract around the hematoma and the projection fibers that connect with other areas of the brain. This could explain why motor deficits were limited to the neurologic deficit score, and involved movement coordination and flexibility with ataxia and gait abnormalities, which are prominent primary symptoms of vascular Parkinsonism. This could indicate that an increase in proinflammatory cytokines aggravates SBI, while an increase in anti-inflammatory cytokines is protective against ICH injury (Chang et al., 2017; Zhu et al., 2019; Li et al., 2021).

We used the NOR and Y-maze tests to assess changes in cognitive function

in the s-ICH and d-ICH models. The NOR test is often used to evaluate recognition memory, attention, anxiety, and preference for novelty in rodents (Barba et al., 2000). The Y-maze test is used to assess short-term memory and spatial memory in mice, and it relies on rodents' innate curiosity to explore previously unvisited areas (Kraeuter et al., 2019). For example, a mouse with intact working memory will remember a familiar object or arms previously visited, and show a preference for approaching a novel object or entering a less recently visited arm. Despite findings of the critical role of the striatum in cognition in rats (Gardner et al., 2020), other studies have failed to find significant learning or memory impairments in rats after striatal ICH (MacLellan et al., 2009). These different results may be related to variable assessment times and hematoma locations used in prior work. Our study revealed that both s-ICH and d-ICH mice exhibited impaired recognition and decreased exploration desire, with more severe deficits in d-ICH mice. Alternation in the Y-maze test did not differ between the four groups, which suggests that spatial memory was not necessarily impaired in the s-ICH and d-ICH groups. However, this result might be due to the fewer entries of ICH mice. Together, our data indicate that d-ICH mice had more severe cognitive impairment than s-ICH mice, which is consistent with clinical findings from patients with recurrent ICH (Pinho et al., 2019). The incidence of vascular cognitive impairment in patients with ICH is approximately 12–27.5% (Laible et al., 2017), but is likely to be significantly higher in patients with recurrent ICH. Cognitive impairment in vascular dementia is a patchy rather than a full-blown decline in all cognitive domains, unlike Alzheimer's disease; this could be reflected by unbalanced damage to cognitive function in our d-ICH model.

We used the open field test to analyze locomotion and anxiety-like behaviors (Sosa et al., 2018; Shi et al., 2021). The average speed was considerably slower in mice with s-ICH or d-ICH than in control mice. There was a significant decline in the average walking speed of the d-ICH mice compared with that of the s-ICH mice. In a 10-minute time period, s-ICH and d-ICH mice exhibited a shorter total distance walked than did the control mice. The total distance walked was shorter in the d-ICH group than in the s-ICH group. These results are similar to a previous study in rats (Cai et al., 2018).

We used the forced swimming test to assess depression-like behaviors (Shi et al., 2021). d-ICH mice had a longer immobility time than s-ICH mice in the forced swimming test, which indicates that d-ICH mice exhibited more severe depression-like behaviors. Post-stroke depression is a common mental disorder associated with increased disability and mortality (Cai et al., 2019), and 20% of ICH survivors have been reported to show clear signs of depression (Koivunen et al., 2015). The inflammatory response promotes SBI (Hua et al., 2020; Ren et al., 2020), increases oxidative stress (Ren et al., 2021), and activates ferroptosis/autophagic cell death pathways (Li et al., 2018; Wan et al., 2019; Weiland et al., 2019), and might be the primary cause of post-ICH depression. The two-stage bilateral ICH model we established had repeated intrastriatal bleeding with enhanced exacerbation of SBI, potentially by the aforementioned mechanisms, which could explain their more severe depression-like behaviors. To our knowledge, none of the current ICH models mimic recurrent ICH. Our novel model will be a valuable tool to study the pathologic mechanisms and therapeutic strategies for recurrent ICH.

The dopaminergic system is associated with depression and movement disorders such as vascular Parkinsonism (Grace, 2016; Poewe et al., 2017). Parkinsonism is a prevalent disease associated with an imbalance in dopamine metabolism. One study has revealed that dopaminergic neurons in the midbrain have bidirectional control capacity (inhibition or excitation); these neurons can immediately and bidirectionally modulate (induce or relieve) multiple independent depression symptoms caused by chronic stress (Tye et al., 2013). Another study showed that stimulation of dopaminergic neurons in the ventral tegmental area of the midbrain regulates motor activity (Jing et al., 2019). Damage to dopaminergic neurons in the distant midbrain has been reported after ICH in the striatum (Chang and Grace, 2014; Yang et al., 2018a). Previous studies have found that ischemic or hemorrhagic damage in the striatum can cause SBI of the substantia nigra after ICH both in patients and in animal models (Fan et al., 2013). Such injuries have been detected by both anatomical and diffusion-weighted magnetic resonance imaging (Yang et al., 2018b). Previous studies have found that ischemic or hemorrhagic damage in the striatum can cause SBI of the substantia nigra after ICH in both patients and animal models (Fan et al., 2013). However, the changes that occur to dopamine neurons in the substantia nigra after bilateral striatum injury are not clear. In our study, we found that the number of dopaminergic neurons tended to decrease in d-ICH mice, which could explain why the locomotor deficits and depression-like behavior were worse in d-ICH mice than in s-ICH mice. Given that no significant loss of dopaminergic neurons was observed in the present study, it is possible that dopaminergic fibers or receptors are instead compromised following recurrent ICH. This could explain why dopamine replacement therapy is ineffective for vascular Parkinsonism (Korczyn, 2015). Recurrent cerebral infarction is one of the most common causes of vascular Parkinsonism in clinical practice. One study showed no substantia nigra damage in 59 of 135 cases with secondary Parkinsonism in patients with multi-infarct encephalopathy (Jellinger, 2001). Vascular Parkinsonism after ICH has rarely been reported. The results of our study suggest that the pathomechanism of vascular Parkinsonism may be associated with dysfunction of the dopaminergic system rather than a decrease in the number of the dopaminergic neurons.

This study has some limitations. First, the aged mice did not have hypertension-related arteriosclerosis. Therefore, this recurrent ICH model does not generate spontaneous bleeding, which differs from clinical ICH. Consequently, the pathologic process of recurrent ICH could perhaps be better simulated in hypertensive mice. Second, the inflammatory response after a single ICH can influence the pathologic process of the second ICH. Thus, the clinical symptoms of recurrent ICH are not the simple addition of the single ICH, and instead exhibit their own unique characteristics. Third, we only used male mice in this study. Due to sex-related differences in behavior, female animals should be included in subsequent research to extend the current results. In future work, we will investigate the pathologic and biochemical changes of brain edema, inflammation, iron toxicity, and ferroptosis, and neurotransmitter alterations after recurrent ICH, as well as explore potential therapeutic strategies. Furthermore, establishing lobar subtypes of the recurrent ICH model will deepen our understanding of recurrent ICH.

In summary, we established and characterized a novel model of recurrent ICH. This model generated reproducible brain damage and expected behavioral changes. This model closely mimics recurrent ganglionic ICH and could represent a novel tool to elucidate its pathogenesis.

Acknowledgments: *We thank Xi Liu (Department of Neurology, The First Affiliated Hospital of Zhengzhou University, China) for help with brain slicing, Yin-Feng Dong (Nanjing University of Chinese Medicine, the Affiliated Hospital of Nanjing University of Chinese Medicine, China) for the randomization of mice, and Yu-Hu Zhang (Department of Neurology, Guangdong Provincial People's Hospital, Guangdong Academy of Medical Sciences, Guangdong Neuroscience Institute, China) for assistance with manuscript preparation.*
Author contributions: *Study conception: LMW, LJW, JW; experiment implementation: LMW, HLR; behavioral data analysis: LPW; other data analysis: ZHL, HMC; manuscript draft: LMW, LJW; manuscript revision: JW. All authors read and approved the final manuscript.*
Conflicts of interest: *The authors declare that they have no conflict of interest.*

References

Aswendt M, Pallast N, Wieters F, Baues M, Hoehn M, Fink GR (2021) Lesion size- and location-dependent recruitment of contralesional thalamus and motor cortex facilitates recovery after stroke in mice. Transl Stroke Res 12:87-97.
Barba R, Martínez-Espinosa S, Rodríguez-García E, Pondal M, Vivancos J, Del Ser T (2000) Poststroke dementia : clinical features and risk factors. Stroke 31:1494-1501.
Boltze J, Aronowski JA, Badaut J, Buckwalter MS, Caleo M, Chopp M, Dave KR, Didwischus N, Dijkhuizen RM, Doeppner TR, Dreier JP, Fouad K, Gelderblom M, Gertz K, Golubczyk D, Gregson BA, Hamel E, Hanley DF, Härtig W, Hummel FC, et al. (2021) New mechanistic insights, novel treatment paradigms, and clinical progress in cerebrovascular diseases. Front Aging Neurosci 13:623751.
Boulouis G, Charidimou A, Pasi M, Roongpiboonsopit D, Xiong L, Auriel E, van Etten ES, Martinez-Ramirez S, Ayres A, Vashkevich A, Schwab KM, Rosand J, Goldstein JN, Gurol ME, Greenberg SM, Viswanathan A (2017) Hemorrhage recurrence risk factors in cerebral amyloid angiopathy: comparative analysis of the overall small vessel disease severity score versus individual neuroimaging markers. J Neurol Sci 380:64-67.
Caeiro L, Ferro JM, Pinho EMT, Canhão P, Figueira ML (2013) Post-stroke apathy: an exploratory longitudinal study. Cerebrovasc Dis 35:507-513.
Cai JC, Liu W, Lu F, Kong WB, Zhou XX, Miao P, Lei CX, Wang Y (2018) Resveratrol attenuates neurological deficit and neuroinflammation following intracerebral hemorrhage. Exp Ther Med 15:4131-4138.
Cai W, Mueller C, Li YJ, Shen WD, Stewart R (2019) Post stroke depression and risk of stroke recurrence and mortality: A systematic review and meta-analysis. Ageing Res Rev 50:102-109.
Casolla B, Moulin S, Kyheng M, Hénon H, Labreuche J, Leys D, Bauters C, Cordonnier C (2019) Five-year risk of major ischemic and hemorrhagic events after intracerebral hemorrhage. Stroke 50:1100-1107.
Chang CF, Cho S, Wang J (2014) (-)-Epicatechin protects hemorrhagic brain via synergistic Nrf2 pathways. Ann Clin Transl Neurol 1:258-271.
Chang CF, Wan J, Li Q, Renfroe SC, Heller NM, Wang J (2017) Alternative activation-skewed microglia/macrophages promote hematoma resolution in experimental intracerebral hemorrhage. Neurobiol Dis 103:54-69.
Chang CH, Grace AA (2014) Amygdala-ventral pallidum pathway decreases dopamine activity after chronic mild stress in rats. Biol Psychiatry 76:223-230.
Charidimou A, Boulouis G, Roongpiboonsopit D, Xiong L, Pasi M, Schwab KM, Rosand J, Gurol ME, Greenberg SM, Viswanathan A (2019) Cortical superficial siderosis and recurrent intracerebral hemorrhage risk in cerebral amyloid angiopathy: Large prospective cohort and preliminary meta-analysis. Int J Stroke 14:723-733.
Charidimou A, Imaizumi T, Moulin S, Biffi A, Samarasekera N, Yakushiji Y, Peeters A, Vandermeeren Y, Laloux P, Baron JC, Hernandez-Guillamon M, Montaner J, Casolla B, Gregoire SM, Kang DW, Kim JS, Naka H, Smith EE, Viswanathan A, Jäger HR, et al. (2017) Brain hemorrhage recurrence, small vessel disease type, and cerebral microbleeds: A meta-analysis. Neurology 89:820-829.

Chen D, Wang J, Xing Y, Jia P, Zhang Y, Wang J, Ren H, Le A, Chen X, Wang J (2020) Behavioral assessment of post-stroke depression and anxiety in rodents. Brain Hemorrhages 1:105-111.
Deng H, Zhang Y, Li GG, Yu HH, Bai S, Guo GY, Guo WL, Ma Y, Wang JH, Liu N, Pan C, Tang ZP (2021) P2X7 receptor activation aggravates NADPH oxidase 2-induced oxidative stress after intracerebral hemorrhage. Neural Regen Res 16:1582-1591.
Fan SJ, Lee FY, Cheung MM, Ding AY, Yang J, Ma SJ, Khong PL, Wu EX (2013) Bilateral substantia nigra and pyramidal tract changes following experimental intracerebral hemorrhage: an MR diffusion tensor imaging study. NMR Biomed 26:1089-1095.
Gardner RS, Gold PE, Korol DL (2020) Inactivation of the striatum in aged rats rescues their ability to learn a hippocampus-sensitive spatial navigation task. Neurobiol Learn Mem 172:107231.
Grace AA (2016) Dysregulation of the dopamine system in the pathophysiology of schizophrenia and depression. Nat Rev Neurosci 17:524-532.
Han X, Lan X, Li Q, Gao Y, Zhu W, Cheng T, Maruyama T, Wang J (2016) Inhibition of prostaglandin E2 receptor EP3 mitigates thrombin-induced brain injury. J Cereb Blood Flow Metab 36:1059-1074.
Han X, Zhao X, Lan X, Li Q, Gao Y, Liu X, Wan J, Yang Z, Chen X, Zang W, Guo AM, Falck JR, Koehler RC, Wang J (2019) 20-HETE synthesis inhibition promotes cerebral protection after intracerebral hemorrhage without inhibiting angiogenesis. J Cereb Blood Flow Metab 39:1531-1543.
He X, Jiang L, Dan QQ, Lv Q, Hu Y, Liu J, Wang SF, Wang TH (2017) Bone marrow stromal cells promote neuroplasticity of cerebral ischemic rats via a phosphorylated CRMP2-mediated mechanism. Behav Brain Res 320:494-503.
Hua W, Chen X, Wang J, Zang W, Jiang C, Ren H, Hong M, Wang J, Wu H, Wang J (2020) Mechanisms and potential therapeutic targets for spontaneous intracerebral hemorrhage. Brain Hemorrhages 1:99-104.
Imamura N, Hida H, Aihara N, Ishida K, Kanda Y, Nishino H, Yamada K (2003) Neurodegeneration of substantia nigra accompanied with macrophage/microglia infiltration after intrastriatal hemorrhage. Neurosci Res 46:289-298.
Jandke S, Garz C, Schwanke D, Sendtner M, Heinze HJ, Carare RO, Schreiber S (2018) The association between hypertensive arteriopathy and cerebral amyloid angiopathy in spontaneously hypertensive stroke-prone rats. Brain Pathol 28:844-859.
Jellinger KA (2001) The pathology of Parkinson's disease. Adv Neurol 86:55-72.
Jia P, He J, Li Z, Wang J, Jia L, Hao R, Lai J, Zang W, Chen X, Wang J (2021) Profiling of blood-brain barrier disruption in mouse intracerebral hemorrhage models: collagenase injection vs. autologous arterial whole blood infusion. Front Cell Neurosci 15:699736.
Jing MY, Han X, Zhao TY, Wang ZY, Lu GY, Wu N, Song R, Li J (2019) Re-examining the role of ventral tegmental area dopaminergic neurons in motor activity and reinforcement by chemogenetic and optogenetic manipulation in mice. Metab Brain Dis 34:1421-1430.
Koivunen RJ, Harno H, Tatlisumak T, Putaala J (2015) Depression, anxiety, and cognitive functioning after intracerebral hemorrhage. Acta Neurol Scand 132:179-184.
Kraeuter AK, Guest PC, Sarnyai Z (2019) The Y-maze for assessment of spatial working and reference memory in mice. Methods Mol Biol 1916:105-111.
Laible M, Horstmann S, Möhlenbruch M, Schueler S, Rizos T, Veltkamp R (2017) Preexisting cognitive impairment in intracerebral hemorrhage. Acta Neurol Scand 135:628-634.
Lan X, Han X, Liu X, Wang J (2019) Inflammatory responses after intracerebral hemorrhage: From cellular function to therapeutic targets. J Cereb Blood Flow Metab 39:184-186.
Lan X, Han X, Li Q, Yang QW, Wang J (2017) Modulators of microglial activation and polarization after intracerebral haemorrhage. Nat Rev Neurol 13:420-433.
Korczyn AD (2015) Vascular parkinsonism--characteristics, pathogenesis and treatment. Nat Rev Neurol 11:319-326.
Li Q, Wang J (2017) Chapter 64- Animal models: cerebral hemorrhage. In: Primer on cerebrovascular diseases (second edition) (Caplan LR, Biller J, Leary MC, Lo EH, Thomas AJ, Yenari M, Zhang JH, eds), pp 306-311. San Diego: Academic Press.
Li Q, Wan J, Lan X, Han X, Wang Z, Wang J (2017a) Neuroprotection of brain-permeable iron chelator VK-28 against intracerebral hemorrhage in mice. J Cereb Blood Flow Metab 37:3110-3123.
Li Q, Lan X, Han X, Durham F, Wan J, Weiland A, Koehler RC, Wang J (2021) Microglia-derived interleukin-10 accelerates post-intracerebral hemorrhage hematoma clearance by regulating CD36. Brain Behav Immun 94:437-457.
Li Q, Weiland A, Chen X, Lan X, Han X, Durham F, Liu X, Wan J, Ziai WC, Hanley DF, Wang J (2018) Ultrastructural characteristics of neuronal death and white matter injury in mouse brain tissues after intracerebral hemorrhage: coexistence of ferroptosis, autophagy, and necrosis. Front Neurol 9:581.
Li Q, Han X, Lan X, Hong X, Li Q, Gao Y, Luo T, Yang Q, Koehler RC, Zhai Y, Zhou J, Wang J (2017b) Inhibition of tPA-induced hemorrhagic transformation involves adenosine A2b receptor activation after cerebral ischemia. Neurobiol Dis 108:173-182.
Li Q, Han X, Lan X, Gao Y, Wan J, Durham F, Cheng T, Yang J, Wang Z, Jiang C, Ying M, Koehler RC, Stockwell BR, Wang J (2017c) Inhibition of neuronal ferroptosis protects hemorrhagic brain. JCI Insight 2:e90777.
MacLellan CL, Langdon KD, Churchill KP, Granter-Button S, Corbett D (2009) Assessing cognitive function after intracerebral hemorrhage in rats. Behav Brain Res 198:321-328.
Manaenko A, Chen H, Zhang JH, Tang J (2011) Comparison of different preclinical models of intracerebral hemorrhage. Acta Neurochir Suppl 111:9-14.
Miedel CJ, Patton JM, Miedel AN, Miedel ES, Levenson JM (2017) Assessment of spontaneous alternation, novel object recognition and limb clasping in transgenic mouse models of amyloid-β and tau neuropathology. J Vis Exp:55523.
Nakase T, Yoshioka S, Sasaki M, Suzuki A (2012) Clinical features of recurrent stroke after intracerebral hemorrhage. Neurol Int 4:e10.
Pasi M, Charidimou A, Boulouis G, Auriel E, Ayres A, Schwab KM, Goldstein JN, Rosand J, Viswanathan A, Pantoni L, Greenberg SM, Gurol ME (2018) Mixed-location cerebral hemorrhage/microbleeds: underlying microangiopathy and recurrence risk. Neurology 90:e119-e126.
Percie du Sert N, Hurst V, Ahluwalia A, Alam S, Avey MT, Baker M, Browne WJ, Clark A, Cuthill IC, Dirnagl U, Emerson M, Garner P, Holgate ST, Howells DW, Karp NA, Lazic SE, Lidster K, MacCallum CJ, Macleod M, Pearl EJ, et al. (2020) The ARRIVE guidelines 2.0: Updated guidelines for reporting animal research. PLoS Biol 18:e3000410.
Pinho J, Costa AS, Araújo JM, Amorim JM, Ferreira C (2019) Intracerebral hemorrhage outcome: A comprehensive update. J Neurol Sci 398:54-66.
Pinho J, Araújo JM, Costa AS, Silva F, Francisco A, Quintas-Neves M, Soares-Fernandes J, Ferreira C, Oliveira TG (2021) Intracerebral hemorrhage recurrence in patients with and without cerebral amyloid angiopathy. Cerebrovasc Dis Extra 11:15-21.
Planton M, Raposo N, Danet L, Albucher JF, Péran P, Pariente J (2017) Impact of spontaneous intracerebral hemorrhage on cognitive functioning: An update. Rev Neurol (Paris) 173:481-489.
Poewe W, Seppi K, Tanner CM, Halliday GM, Brundin P, Volkmann J, Schrag AE, Lang AE (2017) Parkinson disease. Nat Rev Dis Primers 3:17013.
Ren H, Han R, Liu X, Wang L, Koehler RC, Wang J (2021) Nrf2-BDNF-TrkB pathway contributes to cortical hemorrhage-induced depression, but not sex differences. J Cereb Blood Flow Metab 41:3288-3301.
Ren H, Han R, Chen X, Liu X, Wan J, Wang L, Yang X, Wang J (2020) Potential therapeutic targets for intracerebral hemorrhage-associated inflammation: An update. J Cereb Blood Flow Metab 40:1752-1768.
Schneider CA, Rasband WS, Eliceiri KW (2012) NIH Image to ImageJ: 25 years of image analysis. Nat Methods 9:671-675.
Seibenhener ML, Wooten MC (2015) Use of the Open Field Maze to measure locomotor and anxiety-like behavior in mice. J Vis Exp:e52434.
Shi X, Bai H, Wang J, Wang J, Huang L, He M, Zheng X, Duan Z, Chen D, Zhang J, Chen X, Wang J (2021) Behavioral assessment of sensory, motor, emotion, and cognition in rodent models of intracerebral hemorrhage. Front Neurol 12:667511.
Sosa PM, de Souza MA, Mello-Carpes PB (2018) Green tea and red tea from camellia sinensis partially prevented the motor deficits and striatal oxidative damage induced by hemorrhagic stroke in rats. Neural Plast 2018:5158724.
Tsai HH, Chen SJ, Tsai LK, Pasi M, Lo YL, Chen YF, Tang SC, Jeng JS (2021) Long-term vascular outcomes in patients with mixed location intracerebral hemorrhage and microbleeds. Neurology 96:e995-e1004.
Tye KM, Mirzabekov JJ, Warden MR, Ferenczi EA, Tsai HC, Finkelstein J, Kim SY, Adhikari A, Thompson KR, Andalman AS, Gunaydin LA, Witten IB, Deisseroth K (2013) Dopamine neurons modulate neural encoding and expression of depression-related behaviour. Nature 493:537-541.
Veltkamp R, Purrucker J (2017) Management of spontaneous intracerebral hemorrhage. Curr Neurol Neurosci Rep 17:80.
Vidale S, Pini C, Arnaboldi M (2016) Blood pressure control and recurrence of intracerebral hemorrhage. JAMA 315:611.
Wan J, Ren H, Wang J (2019) Iron toxicity, lipid peroxidation and ferroptosis after intracerebral haemorrhage. Stroke Vasc Neurol 4:93-95.
Wang J (2010) Preclinical and clinical research on inflammation after intracerebral hemorrhage. Prog Neurobiol 92:463-477.
Weiland A, Wang Y, Wu W, Lan X, Han X, Li Q, Wang J (2019) Ferroptosis and its role in diverse brain diseases. Mol Neurobiol 56:4880-4893.
Weimar C, Kleine-Borgmann J (2017) Epidemiology, prognosis and prevention of non-traumatic intracerebral hemorrhage. Curr Pharm Des 23:2193-2196.
Weimar C, Benemann J, Terborg C, Walter U, Weber R, Diener HC (2011) Recurrent stroke after lobar and deep intracerebral hemorrhage: a hospital-based cohort study. Cerebrovasc Dis 32:283-288.
Wolf ME, Alonso A, Ebert AD, Szabo K, Chatzikonstantinou A (2016) Etiologic and clinical characterization of patients with recurrent spontaneous intracerebral hemorrhage. Eur Neurol 76:295-301.
Yang J, Li Q, Wang Z, Qi C, Han X, Lan X, Wan J, Wang W, Zhao X, Hou Z, Gao C, Carhuapoma JR, Mori S, Zhang J, Wang J (2017) Multimodality MRI assessment of grey and white matter injury and blood-brain barrier disruption after intracerebral haemorrhage in mice. Sci Rep 7:40358.
Yang Y, Zhang K, Zhong J, Wang J, Yu Z, Lei X, Chen X, Quan Y, Xian J, Chen Y, Liu X, Feng H, Tan L (2018a) Stably maintained microtubules protect dopamine neurons and alleviate depression-like behavior after intracerebral hemorrhage. Sci Rep 8:12647.
Yang Y, Zhang X, Ge H, Liu W, Sun E, Ma Y, Zhao H, Li R, Chen W, Yuan J, Chen Q, Chen Y, Liu X, Zhang JH, Hu R, Fan X, Feng H (2018b) Epothilone b benefits nigrostriatal pathway recovery by promoting microtubule stabilization after intracerebral hemorrhage. J Am Heart Assoc 7:e007626.
Yang Y, Liu ML, Meng RL, Tao T (2022) Expression of PirB and NogoA and neurological deficits in rats with intracranial hemorrhage. Zhongguo Zuzhi Gongcheng Yanjiu 26:3202-3206.
Yankelevitch-Yahav R, Franko M, Huly A, Doron R (2015) The forced swim test as a model of depressive-like behavior. J Vis Exp:52587.
Ye XH, Gao T, Xu XH, Cai JS, Li JW, Liu KM, Song SJ, Yin XZ, Tong LS, Gao F (2018) Factors associated with remote diffusion-weighted imaging lesions in spontaneous intracerebral hemorrhage. Front Neurol 9:209.
Zhang HY, Lu X, Hao YH, Tang L, He ZY (2022) Oxidized low-density lipoprotein receptor 1: a novel potential therapeutic target for intracerebral hemorrhage. Neural Regen Res 17:1795-1801.
Zhang X, Wu Q, Lu Y, Wan J, Dai H, Zhou X, Lv S, Chen X, Zhang X, Hang C, Wang J (2018) Cerebroprotection by salvianolic acid B after experimental subarachnoid hemorrhage occurs via Nrf2- and SIRT1-dependent pathways. Free Radic Biol Med 124:504-516.
Zhang Z, Zhang Z, Lu H, Yang Q, Wu H, Wang J (2017) Microglial polarization and inflammatory mediators after intracerebral hemorrhage. Mol Neurobiol 54:1874-1886.
Zhu H, Wang Z, Yu J, Yang X, He F, Liu Z, Che F, Chen X, Ren H, Hong M, Wang J (2019) Role and mechanisms of cytokines in the secondary brain injury after intracerebral hemorrhage. Prog Neurobiol 178:101610.
Zhu W, Gao Y, Chang CF, Wan JR, Zhu SS, Wang J (2014) Mouse models of intracerebral hemorrhage in ventricle, cortex, and hippocampus by injections of autologous blood or collagenase. PLoS One 9:e97423.
Zhu W, Gao Y, Wan J, Lan X, Han X, Zhu S, Zang W, Chen X, Ziai W, Hanley DF, Russo SJ, Jorge RE, Wang J (2018) Changes in motor function, cognition, and emotion-related behavior after right hemispheric intracerebral hemorrhage in various brain regions of mouse. Brain Behav Immun 69:568-581.

C-Editor: Zhao M; S-Editors: Yu J, Li CH; L-Editors: Cason N, Yu J, Song LP; T-Editor: Jia Y